Volume 10
Number 6
23 June 2023
Pages 1887–2298

Materials Horizons

rsc.li/materials-horizons

ISSN 2051-6347

ROYAL SOCIETY OF CHEMISTRY

COMMUNICATION

Jianguo Guan, Yi Long *et al.*

Physical crosslinked hydrogel-derived smart windows: anti-freezing and fast thermal responsive performance

Materials Horizons

ROYAL SOCIETY OF CHEMISTRY

COMMUNICATION

View Article Online
View Journal | View Issue

Cite this: *Mater. Horiz.*, 2023, **10**, 2004

Received 14th January 2023,
Accepted 22nd March 2023

DOI: 10.1039/d3mh00057e

rsc.li/materials-horizons

Physical crosslinked hydrogel-derived smart windows: anti-freezing and fast thermal responsive performance†

Gang Li,‡[ab] Jiwei Chen,‡[b] Zhaonan Yan,[c] Shancheng Wang,[b] Yujie Ke,[bd] Wei Luo,[a] Huiru Ma,[e] Jianguo Guan *[a] and Yi Long *[bf]

Thermochromic hydrogels are versatile smart materials that have many applications, including in smart windows, sensing, camouflage, *etc.* The previous reports of hydrogel smart windows have been based on covalent crosslinking, requiring multistep processing, and complicated preparation. Moreover, most research studies focused on enhancing the luminous transmittance (T_{lum}) and modulating ability (ΔT_{sol}), while the structural integrity and anti-freezing ability, which are essential in practical applications, have been compromised and rarely investigated. Herein, we develop a new physical (noncovalent crosslinked) hydrogel-derived smart window by introducing an *in situ* free radical polymerization (FRP) of *N*-isopropylacrylamide (NIPAM) in a glycerol–water (GW) binary solvent system. The noncovalent crosslinked PNIPAM GW solutions are facilely synthesized, giving outstanding freezing tolerance (~−18 °C), a comparably high T_{lum} of 90%, and ΔT_{sol} of 60.8%, together with added advantages of fast response time (~10 s) and good structural integrity before and after phase transition. This work could provide a new strategy to design and fabricate heat stimulated smart hydrogels not limited to energy saving smart windows.

New concepts

Though the recently developed hydrogel smart windows have high luminous transmittance and modulating ability, it is still challenging to develop a type of hydrogel smart window with good structural integrity before and after phase transition, antifreezing ability and fast thermal response time by a simple and effective strategy. In this work, we develop a new physical (noncovalent crosslinked) hydrogel-derived smart window by introducing an *in situ* free radical polymerization (FRP) of *N*-isopropylacrylamide (NIPAM) in a glycerol–water (GW) binary solvent system. The precursor solution was directly sandwiched between the glass panels to fabricate the smart windows with an *in situ* preparation method, giving the added benefits of scalability and ability to produce windows with various shapes and sizes. More importantly, a strong cooperative hydrogen bonding between the glycerol and water within the polymeric hydrogel network provides the smart hydrogel with outstanding antifreezing ability and good structural integrity caused by polymerization shrinkage and phase transition shrinkage. The coil-to-globule transitions in real time of the noncovalent crosslinking of PNIPAM indicates an ultra-fast response rate, which is more than an order of magnitude better than those of other hydrogel devices. This new design strategy will be helpful to broaden hydrogel-based applications such as smart windows, sensing, camouflage and anti-counterfeiting.

1. Introduction

Considerable endeavors have been devoted to tackling the excessive energy consumption in buildings as it accounts for approximately 40% of the total energy, while heating, ventilation, and air-conditioning (HVAC) consume half of the energy in buildings.[1–3] Windows are considered as the least energy-efficient part of the building envelope,[4,5] and smart windows aim to improve energy efficiency.

Stimulus-responsive changes that contribute to the dynamical modulation of solar transmission can be utilized for various smart windows,[6] which can be classified as thermochromic, mechanochromic, electrochromic, magnetochromic, photochromic and so forth.[7–10] Among them, thermochromic smart windows have attracted considerable attention due to their low

[a] *State Key Laboratory of Advanced Technology for Materials Synthesis and Processing, International School of Materials Science and Engineering, Wuhan University of Technology, Wuhan 430070, China. E-mail: guanjg@whut.edu.cn*
[b] *School of Materials Science and Engineering, Nanyang Technological University, Singapore, 639798, Singapore*
[c] *Institute of Nanoscience and Nanotechnology, School of Materials and Energy, Lanzhou University, Lanzhou 730000, China*
[d] *Institute of Materials Research and Engineering (IMRE), Agency for Science, Technology and Research (A*STAR), 2 Fusionopolis Way, Innovis #08-03, Singapore 138634, Republic of Singapore*
[e] *School of Chemistry, Chemical Engineering and Life Science, Wuhan University of Technology, Wuhan 430070, China*
[f] *Department of Electronic Engineering, The Chinese University of Hong Kong, New Territories, Hong Kong SAR, China. E-mail: yilong@cuhk.edu.hk*

† Electronic supplementary information (ESI) available. See DOI: https://doi.org/10.1039/d3mh00057e

‡ These authors contributed equally to this work.

Table 1 Summary of some recent thermosensitive hydrogel-based smart windows

Sample	T_{lum} (%)	ΔT_{sol} (%)	Structural integrity across LCST	Antifreezing (°C)	Response time (min)	Ref.
Noncovalent crosslinked viscous PNIPAM GW solutions	89.2	60.8	Good	−18	0.16	This work
Liquid of PNIPAM particles	90	68.1	N. A.	N. A.	15	Zhou *et al.*[15]
P(NIPAM-AEMA)	87.2	81.3	N. A.	N. A.	5	Li *et al.*[14]
Au nanochains-PNIPAM hydrogel	71.2	57.2	N. A.	N. A.	5	Guo *et al.*[17]
covalent crosslinked PNIPAM	70.7	25.5	Poor	N. A.	N. A.	Zhou *et al.*[19]
$V_{0.8}W_{0.2}O_2$@SiO_2/PNIPAM microgels	92.5	77.2	N. A.	N. A.	3	Zhang *et al.*[20]
PNIPAM/AgNW composites	78.3	58.4	N. A.	N. A.	N. A.	Lin *et al.*[21]
PNIPAM-PAM	82.7	38.1	N. A.	N. A.	2	Liu *et al.*[22]
PET/PNIPAM/Cr	68.1	55.2	N. A.	N. A.	3	Fang *et al.*[23]
HPC-PAM-PAA hydrogels	88.7	53.9	N. A.	−5	N. A.	Niu *et al.*[24]

*N. A. not available.

cost, passive light modulation, and zero-energy input.[11] To date, several emerging thermoresponsive materials have been widely studied, including hydrogels, ionic liquids, perovskites, metamaterials, and liquid crystals.[12,13] Thermochromic hydrogels are considered as one of the most cost effective categories and some of the recent research is summarized in Table 1. For example, Li *et al.* reported a new strategy of realizing both large and broadband transmittance modulation by controlling the particle size and internal structure of poly(*N*-isopropylacrylamide-2-aminoethylmethacrylate hydrochloride) (P(NIPAM-AEMA)).[14] Zhou *et al.* developed a high thermal energy storage thermoresponsive hydro-liquid by utilizing the high specific heat of water and the large solar modulation of PNIPAM particles.[15] La *et al.* designed a polyampholyte hydrogel (PAH) based window giving privacy and energy saving functionalities.[16] However, these typical thermosensitive polymeric materials such as PNIPAM and PAH are chemical (covalent crosslinked) hydrogels, which are *ex situ* prepared, requiring multistep processing and complicated preparation and generally have a relatively low thermal response rate.[14–18]

More importantly, the covalent cross-linking network and inhomogeneous structure caused by the cross-linkers may hinder the phase transition of the hydrogels, resulting in possible shrinkage and loss of structural integrity of the smart windows after phase transition, *i.e.* the films become nonuniform and lose coverage in the windows[19] (Fig. 1a). It is worth mentioning that in real applications, anti-freezing is a must but has rarely been investigated (Table 1) and the high-water content makes hydrogels susceptible to freezing, resulting in a loss of smart functionality in the sub-zero temperature and cracks in the windows (Fig. 1a), hazardous to the end users.

In this work, we introduce a new physical (noncovalent crosslinked) hydrogel-derived smart window giving improved freeze tolerance, structural integrity, and an ultra-fast thermal response rate by employing free radical polymerization (FRP) of NIPAM in a glycerol–water (GW) binary solvent system. The influences of polymerization parameters on the LCST and freezing points of the noncovalent crosslinked PNIPAM were investigated in detail. Density functional theory (DFT) analysis is used to investigate the antifreezing mechanisms. The structural integrity of smart windows across phase transition has been researched. This smart window has high luminous transmittance (T_{lum}) of ~90%, high modulating ability (ΔT_{sol}) of 60.8%, ultra-fast response rate, tunable LCST, antifreezing properties, and the excellent ability to maintain structural integrity across the phase transition temperature. The noncovalent crosslinked PNIPAM GW solutions reported herein are expected to broaden the applications in smart hydrogel research, not limited to high-performance energy-efficient smart windows.

2. Results and discussion

Fig. 1b schematically illustrates the concept of the smart windows based on noncovalent crosslinked PNIPAM glycerol–water (GW) solution. The noncovalent crosslinked PNIPAM was synthesized in the GW binary solvent system without adding exogenous cross-linker. Glycerol has wide applications in the fields of chemistry and biology since it can form strong hydrogen bonds with water molecules, which lead to the GW binary solvent showing stronger interactions with the polymers than pure water or glycerol,[25–27] giving reduced LCST and freezing point.[28]

A series of noncovalent crosslinked PNIPAMs were synthesized *via in situ* FRP in the presence of GW binary solvent. The LCST and freezing point were investigated *via* differential scanning calorimetry (DSC), as shown in Fig. 2a–c and Fig. S1–S3 (ESI†). With the weight fraction of glycerol increasing from 0 to 30 wt%, the endothermic peak gradually decreases from 32.7 to 19.1 °C in the heating curve (Fig. 2a and Fig. S1, ESI†) and the exothermic peak gradually decreases from 31.0 to 16.0 °C in the cooling curve (Fig. 2b and Fig. S1, ESI†). These results suggest that the LCST of the noncovalent crosslinked PNIPAM GW solution can be tuned with the amount of glycerol added. Furthermore, the effect of monomer mass fraction on the LCST was studied while keeping the weight ratio of glycerol at 15 wt% (of total GW solvent). With increasing NIPAM mass fraction, the LCST values remains constant (Fig. S2, ESI†), suggesting that the monomer concentration has little effect on the LCST of PNIPAM.[29,30]

As the weight fraction of glycerol increases from 0 to 15 wt%, the storage modulus (G'), loss modulus (G''), and viscosity decrease, while the trend reverses with further increases of glycerol amount (Fig. S4, ESI†), which could be attributed to the

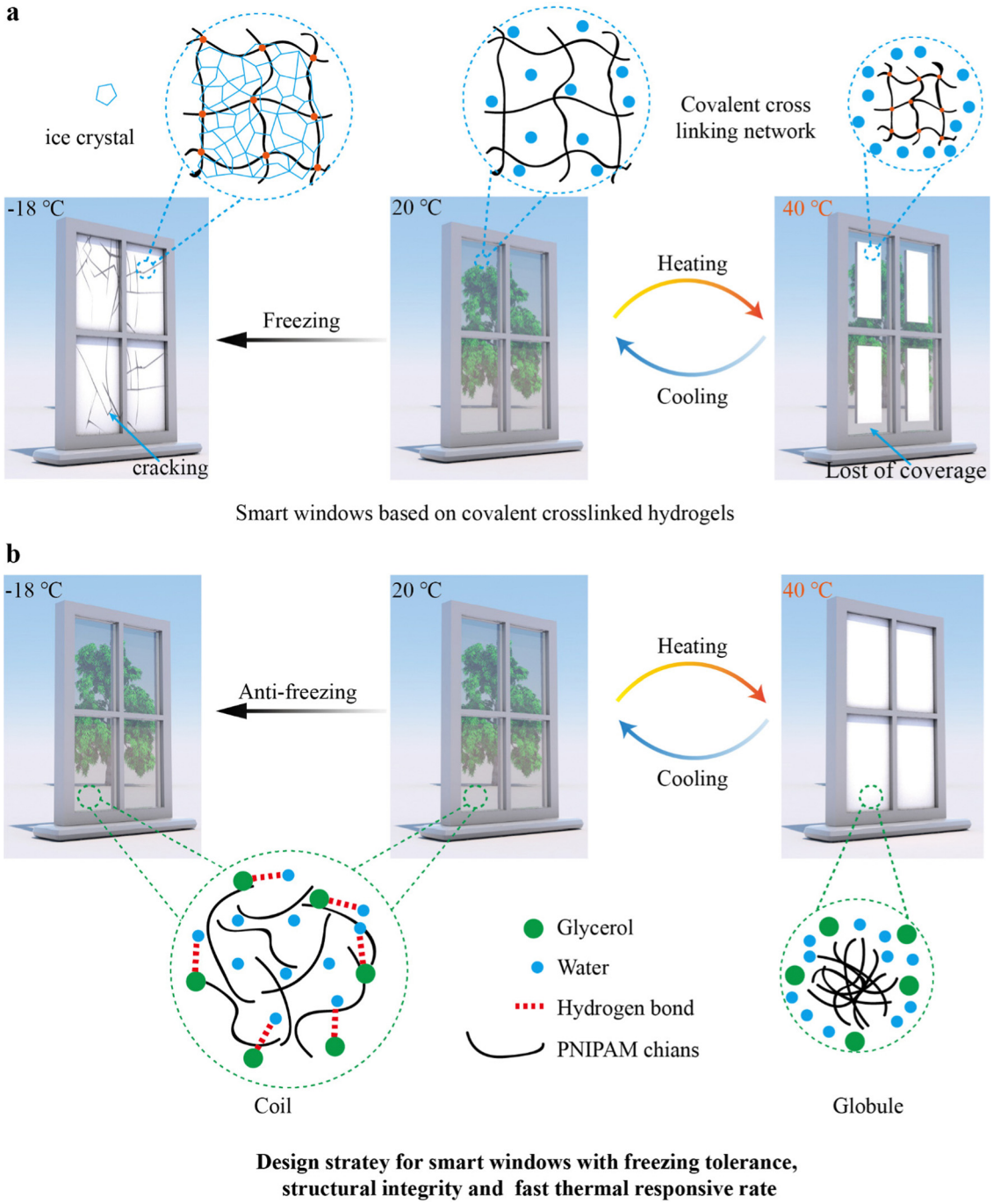

Fig. 1 (a) Common design concepts of smart windows based on covalent crosslinked hydrogel. (b) Concept of the smart windows with freeze tolerance, structural integrity, and ultra-fast thermal responsive rate based on noncovalent crosslinked PNIPAM GW solution.

effects of the interaction between the solvent and polymer. A monotonic increase could be found in the influence of the NIPAM concentration situation on the storage G', G'', and the viscosity (Fig. S5, ESI†) due to the stronger interaction among polymer chains at higher concentrations. To study the temperature effects, temperature sweep measurements were further carried out. Below the LCST, the samples with the glycerol weight ratio ranging from 0 to 25 wt% display sol-like behaviors with a higher G'' than G' (Fig. S6, ESI†), but the 30 wt% glycerol sample turns into gel-like. Above the LCST, an obvious increase in G' was observed, manifesting gel-like behaviors for all samples (Fig. S6, ESI†). A similar phenomenon was observed when increasing the mass fraction of NIPAM from 4.33 to 8.29 wt% (Fig. S7, ESI†).

With the addition weight ratio of glycerol increasing from 0 to 30 wt%, the freezing point decreases as expected (Fig. 2c), as the addition of glycerol disrupts the hydrogen bond network between water molecules and forms a stronger hydrogen bond

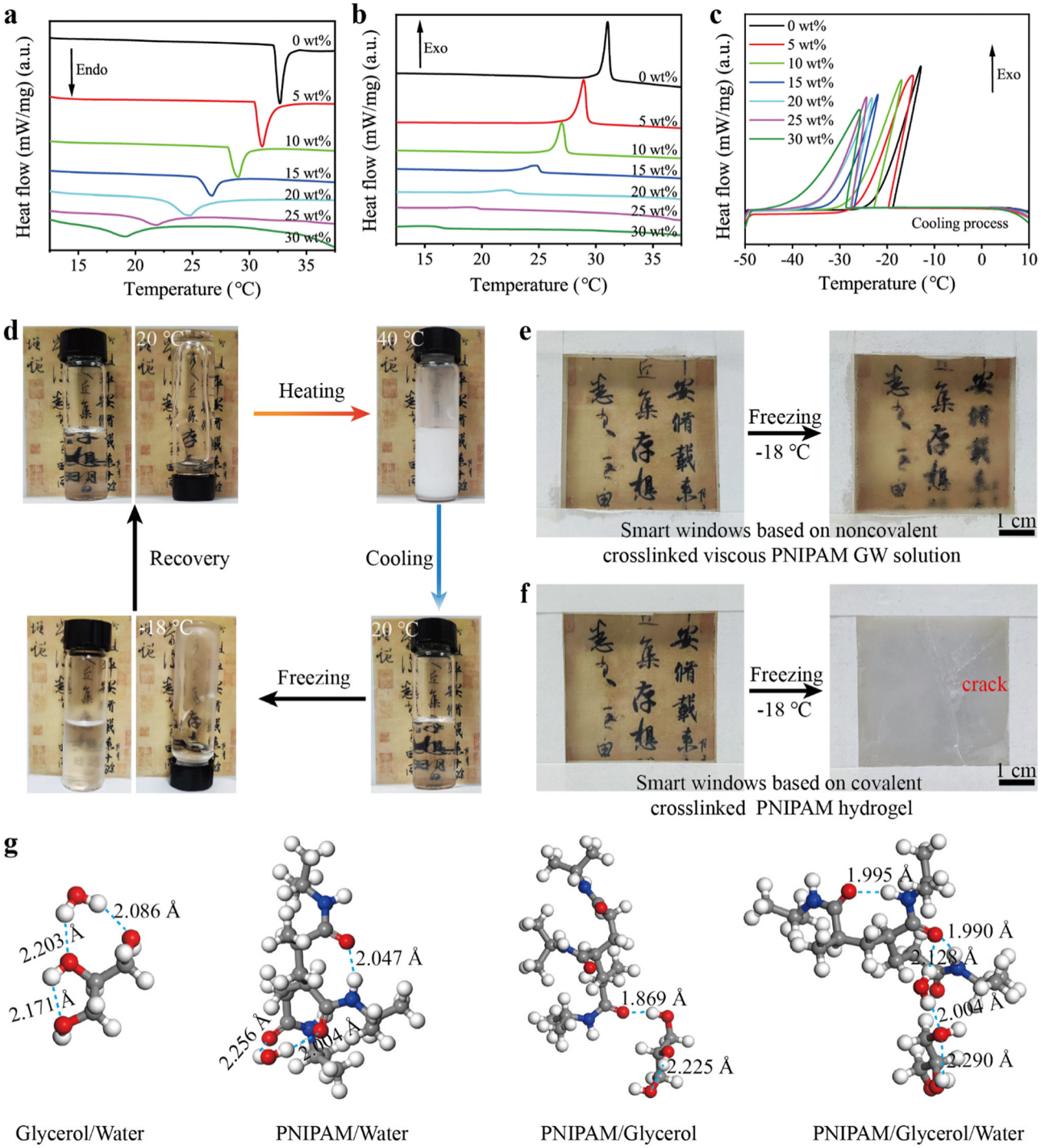

Fig. 2 DSC thermograms of the noncovalent crosslinked PNIPAM prepared with different content of glycerol: (a) heating stage and (b) cooling stage for LCST analysis; (c) for freezing point analysis. (d) The photos of the noncovalent crosslinked PNIPAM GW solutions prepared with 15 wt% glycerol of total solvent after heating, cooling, and freezing. (e) Photos of smart windows based on noncovalent crosslinked viscous PNIPAM GW solutions stored at −18 °C for 3 h. (f) Photos of smart windows based on covalent crosslinked PNIPAM hydrogel stored at −18 °C for 3 h. (g) Density functional theory (DFT) optimized structures and hydrogen bond interactions of glycerol/water, PNIPAM/water, PNIPAM/glycerol and PNIPAM/glycerol/water.

between water–glycerol, which could inhibit the crystallization of water.[31] The 15 wt% glycerol (of the total solvent) and 6.35 wt% NIPAM were selected as the optimal conditions due to the good balance between the LCST, freezing point, and viscosity.

Fig. 2d and Fig. S8–S10 (ESI†) depict the thermochromic performance and anti-freezing performance with noncovalent crosslinked PNIPAM and covalent crosslinked PNIPAM polymerized in GW binary solvent and pure water, respectively. It could be observed that noncovalent crosslinked PNIPAM

synthesized with the GW binary solvent (Fig. 2d) and pure water (Fig. S8, ESI†) are optically transparent, as well as covalent crosslinked PNIPAM synthesized with pure water (Fig. S9, ESI†), while GW binary solvent-synthesized covalent crosslinked PNIPAM is white and opaque (Fig. S10, ESI†). This suggests that the addition of crosslinking agent decreases the solubility of PNIPAM in the GW binary solvent, which may be explained by the higher cross-linking density and the increase of hydrophobicity of the PNIPAM networks.[28] When stored at −18 °C for 3 h, the noncovalent crosslinked PNIPAM prepared with GW binary solvent is not frozen (Fig. 2d). By contrast, both noncovalent crosslinked and covalent crosslinked PNIPAM prepared with pure water solvent have been frozen (Fig. S8 and S9, ESI†). When precursor solutions were sealed between two glass panes to produce sandwich-structured smart windows *via in situ* polymerization, the noncovalent crosslinked PNIPAM GW solution resists freezing due to the presence of glycerol (Fig. 2e), while covalent crosslinked PNIPAM polymerization in pure water was frozen and cracked (Fig. 2f). This could be due to the inflation in volume (8.5%) accompanied by the phase change from water to ice.[32]

To gain further insight into the interactions of glycerol, water, and PNIPAM in the noncovalent crosslinked viscous PNIPAM GW solution, we have calculated the interaction energy using DFT with the Dmol3/GGAPBE/DNP basis set (Fig. 2f). The DFT analysis shows that the interaction energy of the glycerol–water system is lower than that of the water–water system (Table S1, ESI†), confirming that the hydrogen bonding of glycerol–water is more stable than that of the water–water system. Therefore, the introduction of glycerol deceases the freezing point of the noncovalent crosslinked viscous PNIPAM GW solution. The interaction energies of glycerol-PNIPAM and water-PNIPAM are −6.91 and −13.63 kcal mol^{-1}, respectively. Importantly, the interaction energy is reduced to −19.49 kcal mol^{-1} in the glycerol–water-PNIPAM ternary system, demonstrating that the glycerol–water has more hydrogen bonding interactions with the polymers than pure water or glycerol.

For practical applications, the structural integrity and thermal response rate of the designed smart windows are important parameters to be considered.[18,22,33] Herein, we use area percentage to evaluate the structural integrity of the smart windows.

$$\text{Area percentage} = \frac{S}{S_0} \times 100\% \quad (1)$$

where S represents the area of the white and opaque part of the smart windows after heating (the temperature above the LCST), and S_0 is the original area of the transparent region of the smart device before *in situ* reaction. Fig. 3a presents the photos of

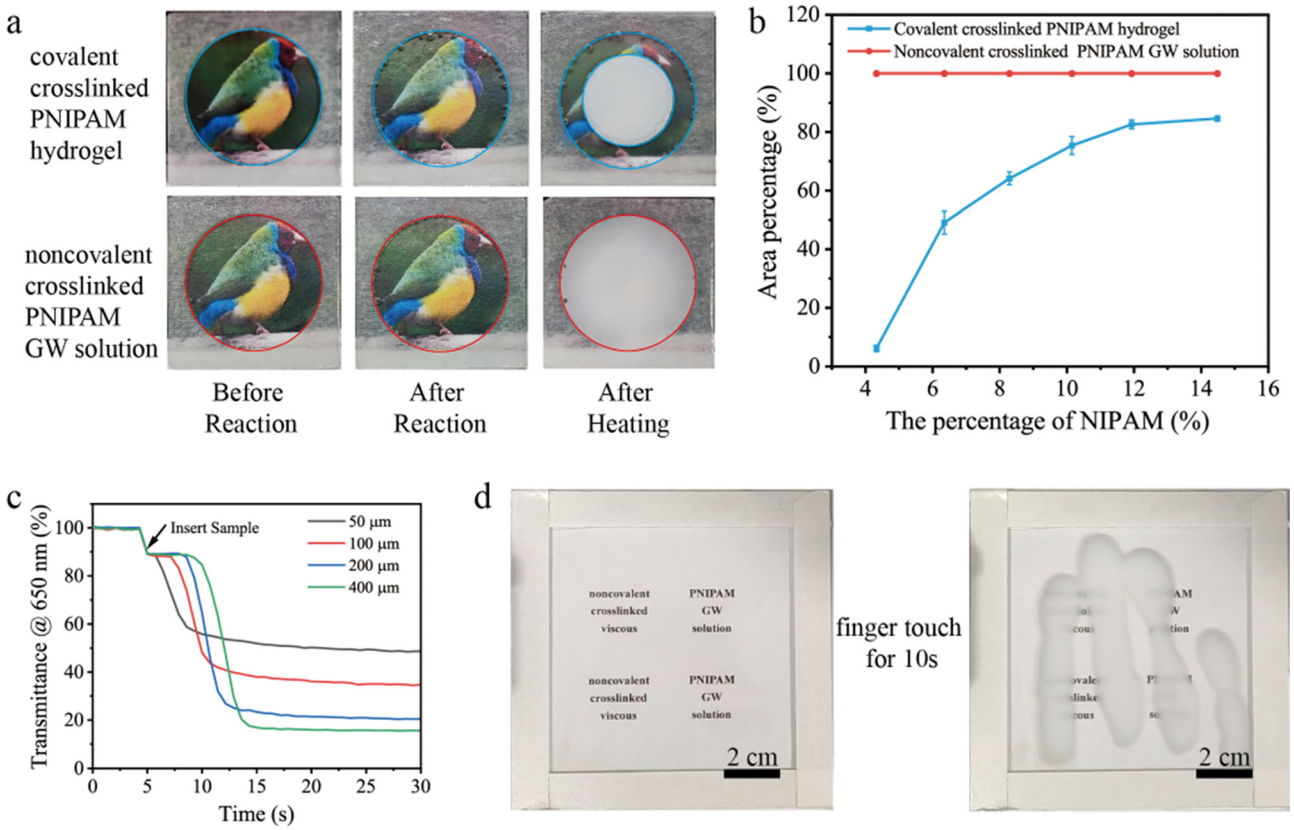

Fig. 3 (a) Photographs of smart windows in different states *via* the *in situ* polymerization. (b) The area percentage curves of the smart windows with the percentage of PNIPAM. (c) The thermal response curves of the noncovalent crosslinked viscous PNIPAM GW solutions with different thickness. (d) The phase transition photographs of the smart window triggered by finger touch. The thickness was 400 μm.

smart windows based on covalent crosslinked PNIPAM and noncovalent crosslinked PNIPAM *in situ* polymerized in pure water and GW binary solvent, respectively. The covalent crosslinked PNIPAM window loses its structural integrity and fails to cover the whole window after heating to 40 °C due to the polymerization shrinkage and phase transition shrinkage, while smart windows based on noncovalent crosslinked PNIPAM GW solutions exhibit structural integrity. In order to clearly evaluate the shrinking behavior, we designed a series of experiments. As can be seen from Fig. 3b and Fig. S11 (ESI†), for the smart window prepared by covalently crosslinked PNIPAM, the area of the white and opaque part is only 6.1% of the original after phase transition when the mass fraction of NIPAM was 4.33%. With the increase of the monomer mass fraction to 14.48%, the area of the white and opaque part increases to 84.6%, but it appears translucent after completing reaction *in situ* polymerization at room temperature (Fig. S11, ESI†). Though reducing the amount of BIS from 1 to 0.5, 0.1 and 0.05 mol% in the synthesis leads to improved structural integrity, the area of the white and opaque regions in the smart windows was still unable to cover the entire surface after phase transition with only 0.05 mol% BIS (Fig. S12, ESI†). On the contrary, in the noncovalent crosslinked counterparts, the area of the white and opaque part remained 100% after phase transition regardless of the monomer fraction (Fig. S13, ESI†).

To measure the thermal response rate, we prepared a measurement device that was equipped with an integration sphere and heating stage (Fig. S14, ESI†). Fig. 3c shows the time dependent transmittance of the noncovalent crosslinked viscous PNIPAM GW solution-based device (2.5 cm × 2.5 cm) with different thicknesses. The T_{lum} of the smart window devices has drastic changes within only 10 s, indicating the ultra-fast response rate, which is more than an order of magnitude better than that of other hydrogel devices (Table 1). This is mainly due to the noncovalent crosslinking of PNIPAM, exhibiting coil-to-globule transitions in real time.[34] For the large-scale sample

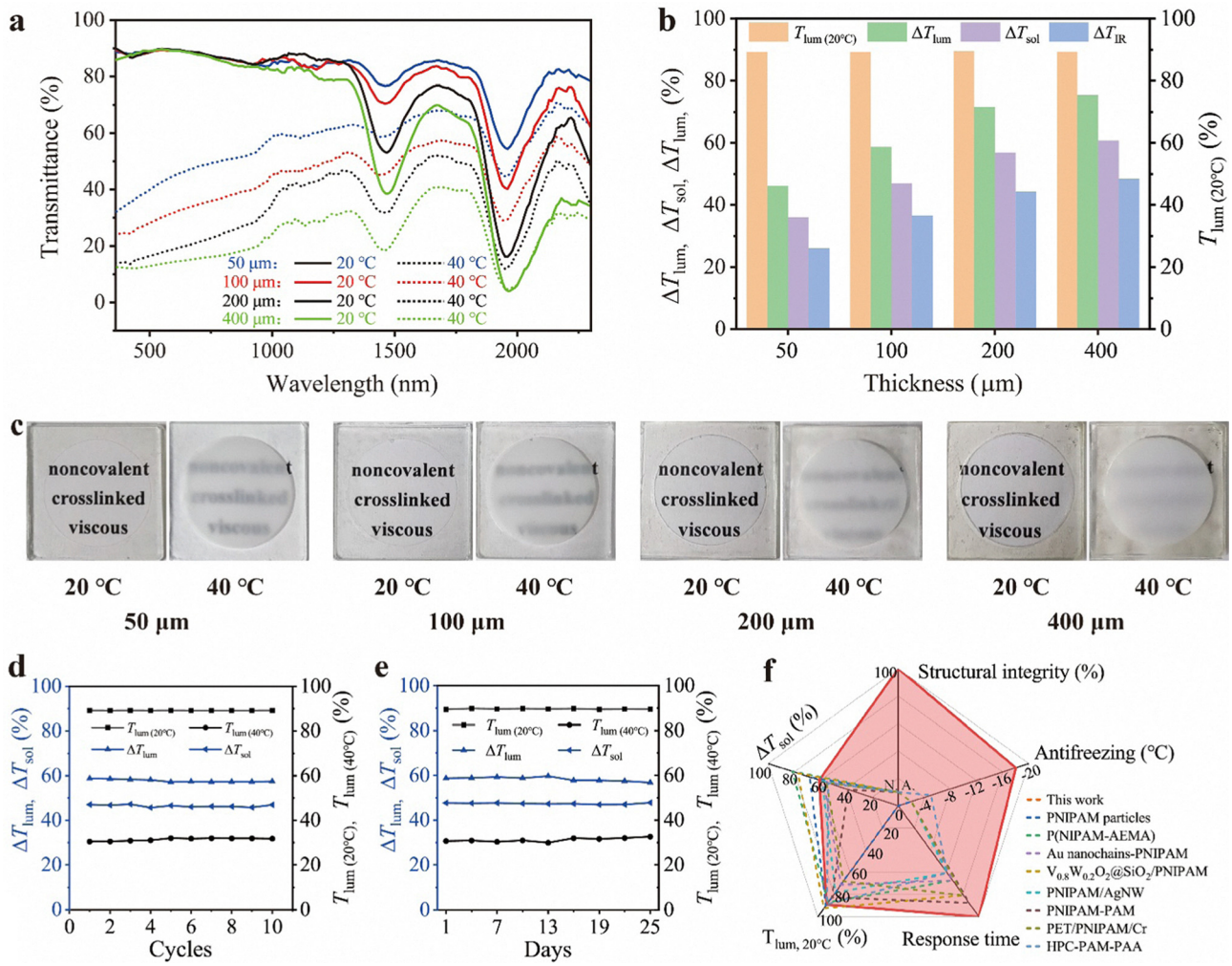

Fig. 4 (a) Transmittance spectra for 50, 100, 200, and 400 μm at 20 °C (solid line) and 40 °C (dashed line), respectively. (b) Comparison of optical performance ($T_{lum,20\ °C}$, ΔT_{lum}, ΔT_{TR} and ΔT_{sol}) for the 50, 100, 200, and 400 μm smart windows. (c) Optical photos for the 50, 100, 200, and 400 μm sample at 20 °C and 40 °C, respectively. Cycling testing (d) and long-term stability testing (e) for the 100 μm sample. (f) Comparison of this work with the recently reported results of covalent crosslinked hydrogel-based thermochromic windows regarding the performance evaluation parameters.

(10 cm × 10 cm), a palm was held on the glass for 10 s and removed, leaving a clear fingerprint on it (Fig. 3d and Movie S1(ESI†)). In conclusion our design of the smart window shows great advantages in the response rate and structural integrity, which will play an important role in real applications.

Fig. 4a shows the transmittance spectra of the noncovalent crosslinked PNIPAM GW samples with thicknesses of 50, 100, 200, and 400 μm at 20 °C and 40 °C, respectively. At 20 °C (lower than LCST), the noncovalent crosslinked PNIPAM chains exist in the coil state, and all the samples show a high luminous transmittance (T_{lum}). While the IR transmittance (T_{IR}) slightly decreases from 83.1% at 50 μm thickness to 73.5% at 400 μm thickness. It can be observed that there exist two sharp absorption peaks at 1400 and 1900 nm; this can be attributed to the water molecule's vibration.[24] As the temperature increases to 40 °C (above LCST), the phase transition induces the lyophilic-to-lyophobic conversion of the PNIPAM network, causing the shrinkage of the polymeric chain to form a scattering center; resulting in opacity for all samples with a decrease in T_{lum}. The calculated optical properties are shown in Fig. 4b. It is readily observed that the modulation of luminous (ΔT_{lum}), IR (ΔT_{IR}), and solar (ΔT_{sol}) gradually grows with the increase of the thickness. For instance, the calculation suggests that ΔT_{lum} increases from 46.1% at 50 μm thickness to 75.5% at 400 μm thickness. Meanwhile, the value changes from 36.1% to 60.8% for ΔT_{sol} and from 26.2% to 48.4% for ΔT_{IR}. These results suggest that the as-obtained smart windows have promising solar modulation ability and the thickness has a significant effect on the ability.

As shown in Fig. 4c, the optical photos for different thickness samples exhibited considerably high transparency and was thickness-independent for luminous transmittance at low temperature (20 °C), and this agrees with the spectra. Upon heating to 40 °C, the samples displayed varying degrees of milky white, and the text under the 400 μm sample even becomes invisible. Therefore, it is concluded that the thermos-responsiveness of the smart windows could be further tuned by varying the temperature and thickness.

To evaluate the ability of the prepared smart window based on noncovalent crosslinked PNIPAM GW solutions to regulate solar light, a control experiment was conducted using clean glass as a reference sample. A test experiment[35] was designed to ensure a stable environment without temperature fluctuations by employing indoor thermal testing. The test box used in the experiment had dimensions of 20 × 20 × 30 cm, and the samples were 10 × 10 cm in size. A heat source in the form of a 50 W heating bulb was placed 15 cm above the sample. The clean glass has an air temperature of 26.7 °C. While the smart window based on noncovalent crosslinked PNIPAM GW solutions has a low air temperature of 25.5 °C (Fig. S15, ESI†). Furthermore, when the PNIPAM filler layer of smart window turns opaque, it reduces the transmittance of solar radiation, resulting in a decline in the rate of temperature increase (Fig. S15, ESI†).

Cycling durability and long-term stability are the key requirements in actual smart window applications. Fig. 4d illustrates the durability test of the 100 μm sample between 20 and 40 °C with 10 cycles. The T_{lum} remained almost constant at both high and low temperatures; moreover, ΔT_{lum} and ΔT_{sol} are also relatively unchanged. Similar results are also observed in the long-term stability test (Fig. 4e). Due to the nonvolatile and low vapor pressure of glycerol, it can preclude the evaporation rate of water from the noncovalent crosslinked PNIPAM GW solutions (Fig. S16, ESI†).

In conclusion our sample displays overall advantages compared with the recently reported results of hydrogel based thermochromic windows (Fig. 4f), including outstanding freezing tolerance (∼−18 °C), fast thermal response rate (∼10 s), a high T_{lum} (90%), a competitive ΔT_{sol} (60.8%) and satisfactory structural integrity after phase transition.

3. Conclusion

In summary, we have demonstrated a new strategy to design and develop a thermochromic smart hydrogel based on the noncovalent crosslinked PNIPAM GW solutions. A strong cooperative hydrogen bonding formed between the glycerol and water within the polymeric hydrogel network has been observed, providing the smart hydrogel with outstanding anti-freezing ability. The physical crosslinking structures give the PNIPAM network an ultra-fast thermal response rate with comparably good thermochromic performances. The *in situ* fabrication avoids the multistep processing and complicated preparation; and this concept of a physical crosslinked hydrogel smart window could maintain the structural integrity across the phase transition, which is often compromised in the covalent bonded counterparts. This new strategy of noncovalent crosslinked hydrogel could facilitate the application of thermochromic devices not limited to smart windows.

4. Experimental section

Materials

N-Isopropylacrylamide (NIPAM, ≥99%, 731129), glycerol (≥99.5%, G9012), *N*,*N*′-methylenebis(acrylamide) (BIS, 99%, crosslinker, 146072), ammonium persulfate (APS, ≥98%, initiator, 248614) and *N*,*N*,*N*′,*N*′-tetramethylethylenediamine (TEMED, 99%, accelerator, T22500) were obtained from Sigma-Aldrich. All chemicals were used as received without further purification. Super-purity water (18.20 MΩ cm) was produced by a Milli-Q system (Millipore, USA). The glass with a thickness of 1.1 mm was purchased from Winteck Technology.

Preparation of the noncovalent crosslinked PNIPAM glycerol–water (GW) solutions

In a typical *in situ* free radical polymerization, an appropriate mass of the NIPAM was first dissolved in deionized water and glycerol binary solvent system according to the special proportion at room temperature. After being entirely dissolved, APS and TEMED were added to the glycerol–water binary solvent,

the mole ratio of APS to NIPAM and TEMED to APS was kept constant at 0.3 : 100 and 3 : 1, respectively. The total weight of GW solvent was 1 g. After reacting for 24 h at room temperature, the noncovalent crosslinked viscous PNIPAM GW solutions could be obtained. For preparing covalent crosslinked PNIPAM hydrogels, 1 mol% BIS (of the NIPAM) was added with other conditions unchanged.

Fabrication of sandwich structure smart windows

The precursor solution was sandwiched between two clean glass slides with a thickness of tens or even hundreds of microns, and with the *in situ* polymerization process, the smart windows based on noncovalent crosslinked viscous PNIPAM GW solutions could be obtained.

Characterization

The UV-Vis-NIR spectra for the sample were measured with the UV-Vis-NIR spectrophotometer system with the integration sphere attached (Avantes AvaSpec-ULS2048L Starline Versatile Fiber-optic Spectrometer and AvaSpec-NIR256-2.5-HSC-EVO). The spectrophotometer is equipped with a heating and cooling stage (Linkam PE120) to control the sample temperature.

The transmittance T_{lum}, T_{TR}, and T_{sol} were calculated using the equation:

$$T_{\mathrm{lum/IR/sol}} = \int \varphi_{\mathrm{lum/IR/sol}} T(\lambda) \mathrm{d}\lambda \Big/ \int \varphi_{\mathrm{lum/IR/sol}} \mathrm{d}\lambda$$

where $T(\lambda)$ is the spectral transmittance (360–780 nm for T_{lum}, 790–2300 nm for T_{IR}, and 360–2300 nm for T_{sol}, respectively). $\varphi_{\mathrm{lum}}(\lambda)$ is the standard luminous efficiency function of photopic vision for the wavelength of 380–780 nm, while $\varphi_{\mathrm{IR}}(\lambda)$ and $\varphi_{\mathrm{sol}}(\lambda)$ are the IR/solar irradiance spectra for air mass 1.5 (corresponding to the sun standing 37° above the horizon with 1.5 atmosphere thickness, corresponding to a solar zenith angle of 48.2°), respectively.

$$\Delta T_{\mathrm{lum/IR/sol}} = T_{\mathrm{lum/IR/sol,20°C}} - T_{\mathrm{lum/IR/sol,40°C}}$$

The LCST and the freezing point of the resulting products were performed on TA Q10 in nitrogen flow over the temperature range of −50 to 45 °C with a heating rate of 2 or 10 °C min^{-1}.

The rheological behaviors of the noncovalent crosslinked viscous PNIPAM GW solutions were analyzed by MCR 302e Rheometer (Anton Paar, Austria) with a 25 mm plane plate. Viscosity was recorded with a shear rate from 0.1 to 100 s^{-1} at room temperature. Frequency sweeps were performed for the solutions with a strain amplitude of 0.5%. Temperature sweeping experiments were conducted with a strain amplitude of 0.5% and a fixed frequency of 1 Hz.

Indoor thermal test

The solar light regulating ability of the prepared smart window based on non-crosslinked PNIPAM GW solutions was assessed in comparison to clean glass through a controlled experiment. The experiment utilized indoor thermal testing to ensure a stable environment without temperature fluctuations. The indoor test box had dimensions of 20 × 20 × 30 cm, with sample sizes of 10 × 10 cm. A heating bulb with a power of 50 W was used as the heat source and placed 10 cm above the sample. Air temperature was measured.

Density functional theory (DFT) study

To gain further insight into the interactions of glycerol, water, and PNIPAM in the system, we carried out density functional theory (DFT) calculations. The simulation was performed using the density functional theory program DMol^3 in Material Studio (Accelrys, San Diego, CA). The physical wave functions were expanded in terms of numerical basis sets, using the Dmol3/GGA-PBE/DNP (3.5) basis set.[36] The core electrons were treated with All Electron. The exchange–correlation energy was treated by the generalized gradient approximation (GGA) with Perdew–Burke–Ernzerhof (PBE).[37,38] A Fermi smearing of 0.005 Ha (1 Ha = 27.211 eV) and a global orbital cutoff of 5.2 Å were employed. The convergence criteria for the geometric optimization and energy calculation were set as follows: (i) a self-consistent field tolerance of 1.0×10^{-6} Ha per atom; (ii) an energy tolerance of 1.0×10^{-5} Ha per atom; (iii) a maximum force tolerance of 0.002 Ha $\mathrm{Å}^{-1}$; (d) a maximum displacement tolerance of 0.005 Å.

Model building

The water molecule interaction model (named W–W model) was built at first and then a glycerol molecule was placed on the water molecule model to investigate the interaction between the water molecule and glycerol molecule (named G–W model). The models of the PNIPAM polymers were composed of 3 monomers. A glycerol molecule was placed on the polymer model to investigate the interaction between glycerol and PNIPAM (named G–PNIPAM model). In the next step, a water molecule was also added to investigate the water effect on PNIAPM (named W–PNIPAM model). Moreover, the interactions among PNIPAM, glycerol and water (named G–W–PNIPAM model) were investigated.

Interaction energy calculation

The intensity of interaction between the components in the system (interaction energy, E_{i}) was described according to the following equation:

$$E_{\mathrm{i}} = E_{\mathrm{t}} - \Sigma E_{\mathrm{c}} \quad (2)$$

where E_{t} and E_{c} represent the total energy of the system, and the energy of each component in the system, respectively. A negative value of interaction energy corresponds to stable adsorption between the components. More negative E_{i} indicates a stronger interaction in the system.

Author contributions

Y. L., J. G. and G. L. conceived the idea. G. L. and J. C. performed most of the experiments and drafted the manuscript.

Z. Y. performed DFT calculations. J. C., Y. K. and S. W. assisted with the characterization. W. L., H. M., J. G. and Y. L. discussed and revised the manuscript. All authors checked the manuscript.

Conflicts of interest

The authors declare no conflict of interest.

Acknowledgements

This work was supported by the National Natural Science Foundation of China (No. 51573144 and 51521001), the Innovation Team in Key Areas of the Innovation Talent Promotion Plan (2021) of MOST, China, and the China Scholarship Council (CSC20200695030). Y. Long is thankful for the funding support from the Ministry of Education Singapore Tier 1 RG71/21, Global STEM Professorship Scheme sponsored by the Government of the Hong Kong Special Administrative Region.

References

1 S. Wang, K. A. Owusu, L. Mai, Y. Ke, Y. Zhou, P. Hu, S. Magdassi and Y. Long, *Appl. Energy*, 2018, **211**, 200–217.
2 S. Zhao, Z. Shao, A. Huang, S. Bao, H. Luo, S. Ji, P. Jin and X. Cao, *Nano Energy*, 2021, **89**, 106297.
3 Y. Ke, Y. Li, L. Wu, S. Wang, R. Yang, J. Yin, G. Tan and Y. Long, *ACS Energy Lett.*, 2022, **7**, 1758–1763.
4 Y. Zhou, X. Dong, Y. Mi, F. Fan, Q. Xu, H. Zhao, S. Wang and Y. Long, *J. Mater. Chem. A*, 2020, **8**, 10007–10025.
5 S. Wang, T. Jiang, Y. Meng, R. Yang, G. Tan and Y. Long, *Science*, 2021, **374**, 1501–1504.
6 J. Li, X. Lu, Y. Zhang, X. Ke, X. Wen, F. Cheng, C. Wei, Y. Li, K. Yao and S. Yang, *Adv. Funct. Mater.*, 2021, **31**, 2102350.
7 Y. Ke, J. Chen, G. Lin, S. Wang, Y. Zhou, J. Yin, P. S. Lee and Y. Long, *Adv. Energy Mater.*, 2019, **9**, 1902066.
8 Y. Zhou, F. Fan, Y. Liu, S. Zhao, Q. Xu, S. Wang, D. Luo and Y. Long, *Nano Energy*, 2021, **90**, 106613.
9 Y. Liu, Q. Fan, G. Zhu, G. Shi, H. Ma, W. Li, T. Wu, J. Chen, Y. Yin and J. Guan, *Mater. Horiz.*, 2021, **8**, 2032–2040.
10 M. Feng, X. Bu, J. Yang, D. Li, Z. Zhang, Y. Dai and X. Zhang, *J. Mater. Sci.*, 2020, **55**, 8444–8463.
11 Y. Ke, Y. Yin, Q. Zhang, Y. Tan, P. Hu, S. Wang, Y. Tang, Y. Zhou, X. Wen, S. Wu, T. J. White, J. Yin, J. Peng, Q. Xiong, D. Zhao and Y. Long, *Joule*, 2019, **3**, 858–871.
12 Y. Ke, C. Zhou, Y. Zhou, S. Wang, S. H. Chan and Y. Long, *Adv. Funct. Mater.*, 2018, **28**, 1800113.
13 Y. Wang, S. Bai, L. Wei, X. Niu, S. Wang, M. Niu, L. Li, X. Guo and Y. Gao, *J. Mater. Sci.*, 2021, **56**, 6955–6965.
14 X.-H. Li, C. Liu, S.-P. Feng and N. X. Fang, *Joule*, 2019, **3**, 290–302.
15 Y. Zhou, S. Wang, J. Peng, Y. Tan, C. Li, F. Y. C. Boey and Y. Long, *Joule*, 2020, **4**, 2458–2474.
16 T.-G. La, X. Li, A. Kumar, Y. Fu, S. Yang and H.-J. Chung, *ACS Appl. Mater. Interfaces*, 2017, **9**, 33100–33106.
17 M. Guo, Q. Yu, X. Wang, W. Xu, Y. Wei, Y. Ma, J. Yu and B. Ding, *ACS Appl. Mater. Interfaces*, 2021, **13**, 5634–5644.
18 L.-W. Xia, R. Xie, X.-J. Ju, W. Wang, Q. Chen and L.-Y. Chu, *Nat. Commun.*, 2013, **4**, 2226.
19 Y. Zhou, Y. Cai, X. Hu and Y. Long, *J. Mater. Chem. A*, 2014, **2**, 13550–13555.
20 R. Zhang, B. Xiang, Y. Shen, L. Xia, L. Xu, Q. Guan and S. Tang, *J. Mater. Chem. A*, 2021, **9**, 17481–17491.
21 C. Lin, J. Hur, Y. H. Chao Christopher, G. Liu, S. Yao, W. Li and B. Huang, *Sci. Adv.*, 2022, **8**, eabn7359.
22 S. Liu, C. Y. Tso, Y. W. Du, L. C. Chao, H. H. Lee, T. C. Ho and M. K. H. Leung, *Appl. Energy*, 2021, **297**, 117207.
23 Z. Fang, L. Ding, L. Li, K. Shuai, B. Cao, Y. Zhong, Z. Meng and Z. Xia, *ACS Photonics*, 2021, **8**, 2781–2790.
24 Y. Niu, Y. Zhou, D. Du, X. Ouyang, Z. Yang, W. Lan, F. Fan, S. Zhao, Y. Liu, S. Chen, J. Li and Q. Xu, *Adv. Sci.*, 2022, **9**, 2105184.
25 Y. Jian, S. Handschuh-Wang, J. Zhang, W. Lu, X. Zhou and T. Chen, *Mater. Horiz.*, 2021, **8**, 351–369.
26 P. Wei, T. Chen, G. Chen, H. Liu, I. T. Mugaanire, K. Hou and M. Zhu, *ACS Appl. Mater. Interfaces*, 2020, **12**, 3068–3079.
27 L. Han, K. Liu, M. Wang, K. Wang, L. Fang, H. Chen, J. Zhou and X. Lu, *Adv. Funct. Mater.*, 2018, **28**, 1704195.
28 M. Wang, Y. Gao, C. Cao, K. Chen, Y. Wen, D. Fang, L. Li and X. Guo, *Ind. Eng. Chem. Res.*, 2014, **53**, 18462–18472.
29 Y. Satokawa, T. Shikata, F. Tanaka, X.-P. Qiu and F. M. Winnik, *Macromolecules*, 2009, **42**, 1400–1403.
30 W. Wang, C. Gao, Y. Qu, Z. Song and W. Zhang, *Macromolecules*, 2016, **49**, 2772–2781.
31 M. Guo, J. Yan, X. Yang, J. Lai, P. An, Y. Wu, Z. Li, W. Lei, A. T. Smith and L. Sun, *J. Mater. Chem. A*, 2021, **9**, 7935–7945.
32 O. Miyawaki, C. Omote, M. Gunathilake, K. Ishisaki, S. Miwa, A. Tagami and S. Kitano, *J. Food Eng.*, 2016, **184**, 38–43.
33 H.-N. Kim and S. Yang, *Adv. Funct. Mater.*, 2020, **30**, 1902597.
34 Y. Alsaid, S. Wu, D. Wu, Y. Du, L. Shi, R. Khodambashi, R. Rico, M. Hua, Y. Yan, Y. Zhao, D. Aukes and X. He, *Adv. Mater.*, 2021, **33**, 2008235.
35 S. Wang, Y. Zhou, T. Jiang, R. Yang, G. Tan and Y. Long, *Nano Energy*, 2021, **89**, 106440.
36 B. Delley, *J. Chem. Phys.*, 2000, **113**, 7756–7764.
37 J. P. Perdew, K. Burke and M. Ernzerhof, *Phys. Rev. Lett.*, 1996, 77, 3865–3868.
38 J. P. Perdew, K. Burke and M. Ernzerhof, *Phys. Rev. Lett.*, 1998, **80**, 891.

